e-ISSN: 2550-164X

Available online at
https://jmeche.uitm.edu.my/

Journal of Mechanical Engineering 22(1) 2025, 17 – 29.

Journal of Mechanical Engineering

Position Tracking Control of an Electromechanical Hip-Knee-Ankle-Foot Orthosis

Zulkiffli Abd Kadir[1*], Muhammad Akhmal Hakim Alias[1],
Aina Nabila Azman[1], Khisbullah Hudha[1]

[1]*Department of Mechanical Engineering, Faculty of Engineering, Universiti Pertahanan Nasional Malaysia, Sungai Besi, Kuala Lumpur, Malaysia*

ARTICLE INFO

Article history:
Received 07 March 2024
Revised 25 March 2024
Accepted 27 August 2024
Online first
Published 15 January 2025

Keywords:
Walking aid
Double pendulum
Electromechanical hip-knee-ankle-foot orthosis

DOI:
10.24191/jmeche.v22i1.4553

ABSTRACT

The walking ability of the elderly is a major global health concern. Most of the elderly experience walking difficulties such as decreased walking speed and loss of balance as well as coordination. To address this issue, a mechanical orthosis called the hip-knee-ankle-foot orthosis (HKAFO) has been designed to assist elderly individuals and hospital patients in performing therapeutic treatments. However, the existing standard HKAFOs have several limitations including high energy consumption and overloading of the hip and lower limb joints during walking activities. Therefore, this study aims to enhance the standard HKAFO by developing an electromechanical HKAFO (EM-HKAFO). The study involves developing a two-degree-of-freedom mathematical model of a double pendulum using Lagrange formulation to represent the HKAFO structure and evaluate the kinematic motions of the lower limbs. The performance of the proposed walking aid is evaluated using an actual instrumented EM-HKAFO focusing on its effectiveness in achieving a desired walking angle of 25º. The result indicates that the difference between simulation and experimental data is within an acceptable error range of 14%. Overall, this study contributes to the advancement of mobility aids and enhances the quality of life for elderly individuals and patients in need.

INTRODUCTION

Patients who experience lower limb weakness often encounter difficulties performing basic movements like walking and standing up without assistance. This places both the patient and the helper under pressure, and there is a high risk of falling and injury. To assist patients in performing these movements, conventional walking aids such as exoskeletons and orthoses have been developed. Wearable devices like exoskeletons (Yan et al., 2021; Tang et al., 2022) and orthoses (Kobayashi et al., 2019) have been researched to help patients regain strength in their limbs, enabling them to stand and walk normally (Cao et al., 2021; Ataabadi et al., 2022). However, these aids require a significant amount of energy to transfer force from the feet to the entire lower limbs. To overcome this challenge, a robotic mechanism has been designed by integrating it with conventional walking aids. This integration provides stability, balance, and power, as patients have

[1*] Corresponding author. *E-mail address*: zulkiffli@upnm.edu.my
https://doi.org/10.24191/jmeche.v22i1.4553

limited control over their lower limbs. Notable rehabilitation technologies (Shi et al., 2019; Huamanchahua et al., 2021; Wang et al., 2022; Khalid et al., 2024) have been developed worldwide by institutions, universities, and industries.

Common issues with previous exoskeleton designs include limited range of motion, lack of adaptability to various tasks, wearer discomfort, inefficiency in power consumption, and controller limitations. Many exoskeletons restrict degrees-of-freedom, impeding natural movement and task performance. This limitation can particularly hinder activities requiring intricate movements or precise motor control. Comfort poses a significant challenge as exoskeletons often involve bulky structures, rigid materials, and poorly distributed weight, potentially causing discomfort and musculoskeletal issues with prolonged use. Complex control interfaces or the need for extensive user training further complicate matters, acting as barriers to adoption and limiting usability.

A research study focused on a robotic exoskeleton with six actuated joints, utilizing DC brushless motors. This exoskeleton incorporated a gearbox and was developed for both legs, including the hip, knee, and ankle joints (Bortole et al., 2015). The control algorithm, strain gauges, and torque sensors were used to provide complete gait movement. The exoskeleton's overall weight, including the battery and aluminium structure, was 12 kg. In 2016, Gan et al. (2016) developed a lightweight rehabilitation exoskeleton robot weighing 11.6 kg. Their focus was on the patient's freedom of balance and movement. The exoskeleton consisted of one degree-of-freedom (DOF) for the pelvic area and 4 DOFs for the thighs and legs, utilizing a movement locus of direction approach. The lengths of the thigh and torso were adjustable to accommodate different patients. The exoskeleton was actuated using a Maxon flat motor with a Harmonic Drive gearbox having a 160:1 ratio. Additionally, an inertia measurement unit served as a sensory system.

As the effort to design less patient interaction force, Jin et al. (2017) developed an exoskeleton that improved tracking performance. The design comprised two subsystems: the first subsystem tracked the motion phase, and the second subsystem tracked the velocity. Various sensors, such as force-sensing resistors and ribbon switches, were attached to translate the intended motion phase of the patient. An adaptive fuzzy sliding mode controller was developed to control the exoskeleton for two units of powered anthropomorphic legs with 7 DOFs in the lower limb. A study conducted at the Chinese University of Hong Kong (CUHK) developed an exoskeleton to assist paralysis patients in performing sit-to-stand (STS) and gait movements (Chen et al., 2017). The exoskeleton was based on a seven degree-of-freedom (7-DOF) motion for both legs and incorporated additional safety features using mechanical stoppers. Each joint of the hip and knee utilized a DC motor equipped with a Maxon-designed planetary gearbox to provide the appropriate torque for movement. The exoskeleton was equipped with various sensors, including encoders, potentiometers, inertia measurement units, and force sensors. The system employed one PC, two 16-MHz Arduino Micro microcontrollers, and two 84-MHz Arduino DUE microcontrollers for data processing and communication, which were connected via a Bluetooth module. The overall weight of the CUHK exoskeleton was 22 kg, including a set of lithium batteries capable of running up to 3 hours.

Another exoskeleton called the EKSO GT Exoskeleton (Ekso Bionics, 2024) was developed by an American company for gait rehabilitation purposes. This exoskeleton featured six degrees-of-freedom (6-DOF) on both legs, with actuation at the hip and knee joints, while the ankle joints were designed as passive systems. The exoskeleton worked in conjunction with smart Variable Assist software, allowing patients to adjust the assistive energy needed during walking. Next, ongoing research in the field of lower limb walking aids continues to explore designs that can provide the appropriate walking pace for specific patient conditions (Gao et al., 2022; Mayag et al., 2022; Li et al., 2022). While the walking aid has shown successful results in patient testing, several improvements could be further explored in terms of modern shape, compact size, lightweight design, and comfortability. These improvements would provide users with a more natural leg-wearing experience (Abdul Saad et al., 2017; Barrera et al., 2022).

In this study, a compact robotic orthosis namely electromechanical hip-knee-ankle-foot orthosis (EM-HKFO) is developed by identifying the correlation of the patient’s walking activity towards the hip angle

https://doi.org/10.24191/jmeche.v22i1.4553

using a single actuator. The proposed system addresses key drawbacks, primarily complex control interfaces and the need for extensive user training to operate effectively. The proposed EM-HKAFO controller utilizes a switching mechanism, making it user-friendly for both the user and assisting personnel. By incorporating an actuator at the hip joint connected to the knee joint, the EM-HKAFO efficiently generates walking force while facilitating a smoother transfer of force to the lower limbs. Additionally, this design facilitates a more efficient transfer of force to the lower limbs. The proposed solution aims to reduce the dependency on helpers and provide patients with a safe and reliable method of performing basic movements. By using EM-HKAFO, patients can benefit from the stability and balance provided by the robotic mechanism, allowing them to perform activities with greater ease and reducing the risk of falling and getting injured. Besides, this study aims to develop an innovative solution that can enhance the quality of life for patients with lower limb weakness and improve their overall mobility.

Mathematical model of two degree-of-freedom of double pendulum using Lagrange formulation

The double pendulum model is commonly utilized to represent the hip and knee mechanisms in exoskeletons and human walking analysis. In this study, the dynamic motion of the exoskeleton is modeled using a Lagrange approach based on the double pendulum mechanism, as shown in Fig 1(a). This model consists of two interconnected pendulums that represent the thigh and shank segments of the leg. The thigh pendulum is connected to the body at the hip joint, while the shank pendulum is connected to the thigh pendulum at the knee joint.

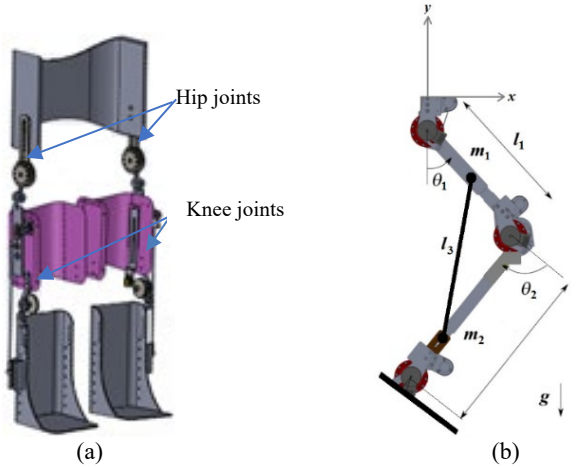

Fig. 1. Double pendulum used to model the dynamic effects using Lagrange formulation; (a) exoskeleton design and (b) double pendulum for the exoskeleton.

An additional link (l_3) is attached between the thigh and shank to make the overall exoskeleton system able to be operated with a single actuator. In the modeling process, several assumptions are made. During the swing phase of gait when the leg is in the air, the double pendulum is treated as a hanging pendulum with the hip joint fixed. Conversely, during the stance phase when the leg is in contact with the ground, the double pendulum transforms into an inverted pendulum, with the ankle joint serving as the pivot point. By referring to the double pendulum mechanism in Fig 1(b), θ_1, m_1, and l_1 are the angle, mass, and length of the thigh, respectively. Meanwhile, θ_2, m_2, and l_2 are the angle, mass, and length of the shank, respectively. Lastly, g is the acceleration due to gravity. The authors have previously conducted a detailed validation procedure for this model, as referenced in Kadir et al. (2023). The equations of motion for the exoskeleton using a double pendulum are derived using the Lagrangian formulation. Generally, the Lagrangian is a

https://doi.org/10.24191/jmeche.v22i1.4553

mathematical function that describes the difference between the kinetic and potential energies that can be written as follows:

$$L = T - U \tag{1}$$

where T represents the total kinetic energy and U represents the total potential energy of the mechanism. The kinetic energy T of the double pendulum is the sum of the kinetic energy of each pendulum. Similarly, the potential energy U is the sum of the potential energy of each pendulum. The total kinetic and potential energies can be written as:

$$T = \frac{1}{2} m_1 \left(\dot{x}_1^2 + \dot{y}_1^2\right) + \frac{1}{2} m_2 \left(\dot{x}_2^2 + \dot{y}_2^2\right) \tag{2}$$

$$U = m_1 g y_1 + m_2 g y_2 \tag{3}$$

Here, y_1 and y_2 are the positions of both thigh and shank in the y-axis, meanwhile $\dot{x}_1, \dot{x}_2, \dot{y}_1$ and $\dot{y}_2$ are the respective velocities at the x and y axes. All the positions and velocities can be written as:

$$x_1 = l_1 \, sin \, sin \, \theta_1 \qquad y_1 = -l_1 \, cos \, cos \, \theta_1 \tag{4}$$

$$x_2 = l_1 \, sin \, sin \, \theta_1 + l_2 \, sin \, sin \, \theta_2 \quad y_2 = -l_1 \, cos \, cos \, \theta_1 - l_2 \, cos \, cos \, \theta_2 \tag{5}$$

$$\dot{x}_1 = \dot{\theta}_1 l_1 \, cos \, cos \, \theta_1 \qquad \dot{y_1} = \dot{\theta}_1 l_1 \, sin \, sin \, \theta_1 \tag{6}$$

$$\dot{x}_2 = \dot{\theta}_1 l_1 \, cos \, cos \, \theta_1 + \dot{\theta}_2 l_2 \, cos \, cos \, \theta_2 \quad \dot{y_2} = \dot{\theta}_1 l_1 \, sin \, sin \, \theta_1 + \dot{\theta}_2 l_2 \, sin \, sin \, \theta_2 \tag{7}$$

Next, by replacing Equation (2) and Equation (3) with Equation (1), the Lagrange mathematical function is written as follows:

$$L = T - U = \frac{1}{2} m_1 l_1^2 \, \dot{\theta}_1^2 + \frac{1}{2} m_2 \left(l_1^2 \, \dot{\theta}_1^2 + l_2^2 \, \dot{\theta}_2^2 + 2 l_1 l_2 \dot{\theta}_1 \dot{\theta}_2 \, cos \, cos \, (\theta_1 - \theta_2)\right) + (m_1 + m_2) g l_1 \, cos \, cos \, \theta_1 - m_1 g l_2 \, cos \, cos \, \theta_2 \tag{8}$$

After that, the equation of motion for Lagrange formulation is used to find the equation for the angles. The general equation of motion is written as:

$$\frac{d}{dt}\left(\frac{\partial L}{\partial q_i}\right) - \frac{\partial L}{\partial q_i} = Q_i \tag{9}$$

By applying the equation of motion, final equations for both hip and knee angles are derived. These equations are expressed as Equation (10) represents the final equation of motion for the hip angle, while Equation (11) corresponds to that of the knee angle, where T_m is the input torque of the system.

$$\ddot{\theta}_1 = \frac{T_m - m_2 l_1 l_2 \ddot{\theta}_2 \, cos \, cos \, (\theta_1 - \theta_2) - (m_1 + m_2) g l_1 \, sin \, sin \, \theta_1 - m_2 l_1 l_2 \dot{\theta}_2^2 \, sin \, sin \, (\theta_1 - \theta_2)}{(m_1 + m_2) l_1^2} \tag{10}$$

https://doi.org/10.24191/jmeche.v22i1.4553

$$\ddot{\theta}_2 = \frac{0.51T_m + m_2 l_1 l_2 \dot{\theta}_1^2 \, sin\, sin\, (\theta_1 - \theta_2) \; - m_1 l_2 g \, sin\, sin\, \theta_2 \; - m_2 l_1 l_2 \ddot{\theta}_1 \, cos\, cos\, (\theta_1 - \theta_2)}{m_2 l_2^2} \tag{11}$$

Development of DC motor controller by simulation

DC motor modelling is a fundamental aspect of designing control systems for various industrial applications. Numerous studies have been conducted on DC motor modelling and control, aiming to understand the dynamic behaviour of the system using circuit theory and mathematical models. In this study, the DC motor is used as the exoskeleton actuator. DC motor is considered in this study as compared to other actuators such as pneumatic, hydraulic, and piezoelectric because of its capability to produce high torque and speed as well as limited space around the joint. A DC motor can be defined as any of a class of rotary electrical motors that converts direct current (DC) electrical energy into mechanical energy (Emhemed & Mamat, 2012; Geonea & Tarnita, 2017). The electric circuit of the armature and the free-body diagram of the rotor are shown in the following Fig 2.

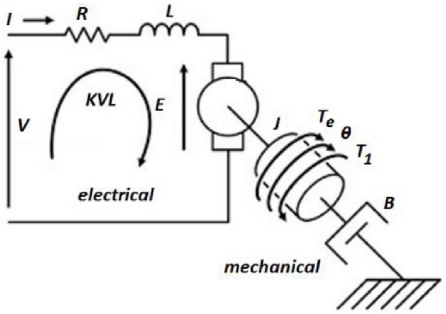

Fig. 2. DC motor equivalent circuit.

From Fig 2, a mathematical model of the DC motor can be derived as:

$$-V + E + RI + L\frac{d}{dt}I = -V + E + RI + sLI = 0 \tag{12}$$

where V is voltage, E is back electromagnetic voltage, R is resistor, L is inductance, and I is current. The current produced by the DC motor is simplified as:

$$I = \frac{1}{sL+R}(V - E) \tag{13}$$

The current produced by the DC motor is then used to investigate the dynamics of the mechanical part namely the mechanical shaft which rotates at its axis with a column friction damper. Based on the Second Newton's Law, the total moment of the shaft axis is derived as:

$$T_e - B\dot{\theta} - T_1 = J\frac{d}{dt}\dot{\theta} \tag{14}$$

https://doi.org/10.24191/jmeche.v22i1.4553

By using the Laplace function, the motor torque can be obtained as:

$$T_e = J\frac{d}{dt}\dot{\theta} + B\dot{\theta} + T_1 = sJ\dot{\theta} + B\dot{\theta} + T_1 \tag{15}$$

where T_e is motor torque, B is damper constant, T_1 is reaction torque, L is the rotational moment of inertia, and $\dot{\theta}$ is angular rate. Finally, the angular velocity of the DC motor can be written as:

$$\dot{\theta} = \frac{1}{sJ + B}(T_e - T_1) \tag{16}$$

The relationship between current and motor torque, the angular rate for the mechanical part and back electromagnetic can be written as:

$$T_e = K_t I \tag{17}$$

$$E = K_e\dot{\theta} \tag{18}$$

where K_t is the constant value for electrical parts and K_e is the constant value for mechanical parts. The equations of motion of the electrical and mechanical parts that have been derived are then merged and developed using MATLAB-Simulink environment as illustrated in Fig 3. The parameters of the DC motor model are $L = 0.1, R = 0.5, K_t = 1.6, K_e = 1.6, J = 5,$ and $B = 0.01$.

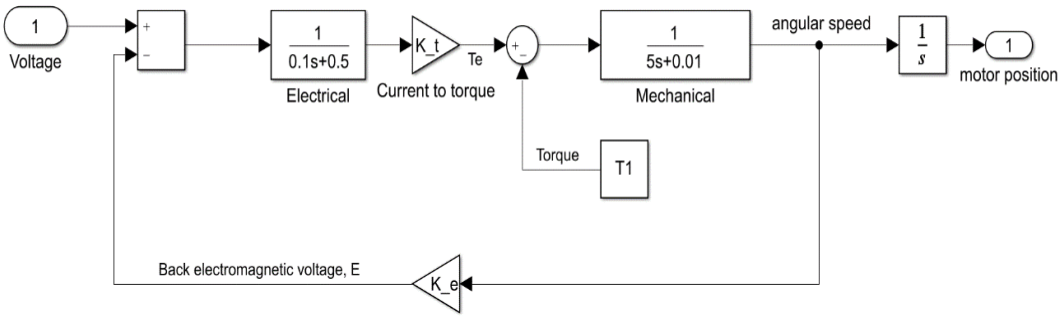

Fig. 3. DC motor model.

The developed DC motor model is then used to form a controllable DC motor system. The position tracking control of the DC motor using the PID controller is developed as illustrated in Fig 4. The purpose of the simulation work in position tracking control is to get the initial parameters of the controller which can minimize the parameter tuning during the experimental work. In the next section, position tracking control of the DC motor by experiment is performed to validate the modeling parameters as well as the control parameters.

https://doi.org/10.24191/jmeche.v22i1.4553

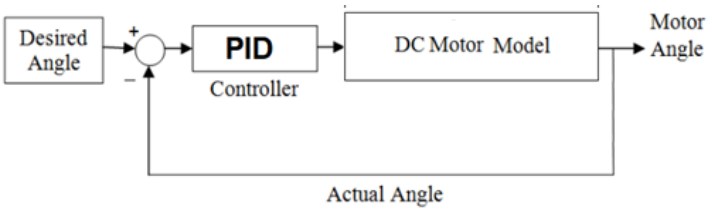

Fig. 4. Position tracking controller of DC motor model.

Experimental setup and validation result for position tracking control of DC motor

Fig 5 shows the experimental setup for position tracking control of the DC motor. The setup consists of several components namely Arduino Uno microcontroller, motor driver MDD10A, and 3000mAh LiPo battery. The Arduino Uno is connected to the Arduino IDE software to run the motor based on a coding script. In addition, a rotary encoder as an angle sensor is also installed for capturing the actual angle of the DC motor. The angle sensor measures the rotational position of the DC motor. This sensor plays a crucial role in the closed-loop control system, ensuring the motor operates according to the desired angle value.

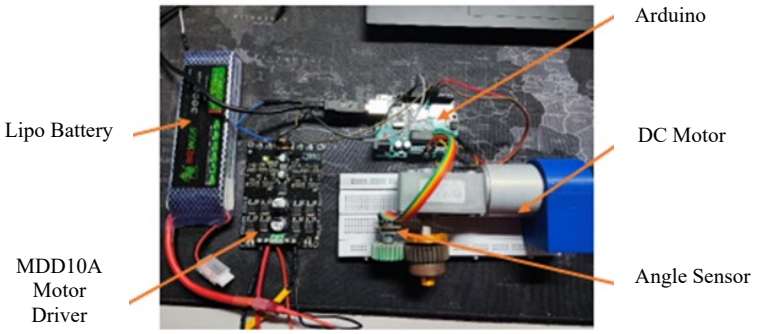

Fig. 5. Experimental setup for position tracking control for DC motor.

Next, the result of the DC motor position tracking control using PID is evaluated by comparing both simulation and experimental responses against the desired angle of 0.436 rad (25º) within 10 seconds. From the results as presented in Fig 6, it can be seen that the simulation model managed to closely track the desired magnitude with a magnitude of 0.44 rad resulting 0.9% error as compared to the desired angle. Minor time delay also can be observed from the simulation result, however the delay is still within the acceptable range. When moving to the experimental result, 0.48 rad of angle is recorded where resulting 10% error against the desired angle. Several factors may contribute to this difference between the desired and measured angles. It could be due to the sensor delay and limitations in the control algorithm employed. These factors can contribute to imprecisions that affect the accuracy of the angle measurement.

Development of switching controller for EM-HKAFO

A switching controller can be used to control a DC motor using different control strategies based on specified conditions. By incorporating the '*switch*' block along with control logic blocks, a dynamic control system can be developed. In this study, the control strategy uses a manual operator to control the actuators. Then, the PID controller is used to regulate the DC motor's angular position. The '*switch*' block acts as the toggle switch, determining which control strategy to enable or disable based on the conditions set in the control logic. In the simulation, the toggle switch will switch the operation of two control strategies for

https://doi.org/10.24191/jmeche.v22i1.4553

both left and right legs, allowing the DC motor to change the movement which acts as normal human movements. This approach provides a flexible and efficient way to manage the DC motor, enhancing its functionality and applicability in diverse applications.

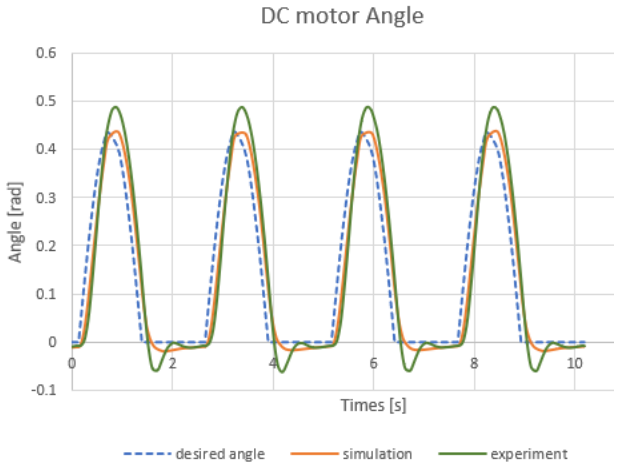

Fig. 6. The simulation and experimental results of the DC motor against the desired angle.

Fig 7 shows a block diagram of a controller and actuator with the exoskeleton as a plant. In the inner loop control system comprising a PID controller, a DC motor acting as an actuator, and an exoskeleton as the plant, the block diagram represents the flow of control signals and feedback. It is important to note that the exoskeleton model in this study has been validated using experimental data, as detailed in the author's previous manuscript (Kadir et al., 2023). The set point, which denotes the desired reference value, is used as input feeds into the PID controller. This controller, utilizing feedback from a sensor that measures the DC motor's actual output, calculates an appropriate control signal. The control signal is then transmitted to the DC motor, which acts as the actuator, converting the signal into physical motion to drive the exoskeleton. The exoskeleton, serving as the plant in this system, responds to the control input from the actuator. Although the exoskeleton operates in an open-loop manner, the PID controller relies on feedback from the sensor to continually adjust the control signal, ensuring the exoskeleton's performance aligns with the desired set point. Through this closed-loop mechanism, the PID controller precisely guides the DC motor's actions, leading to accurate and controlled movements in the exoskeleton for optimal performance.

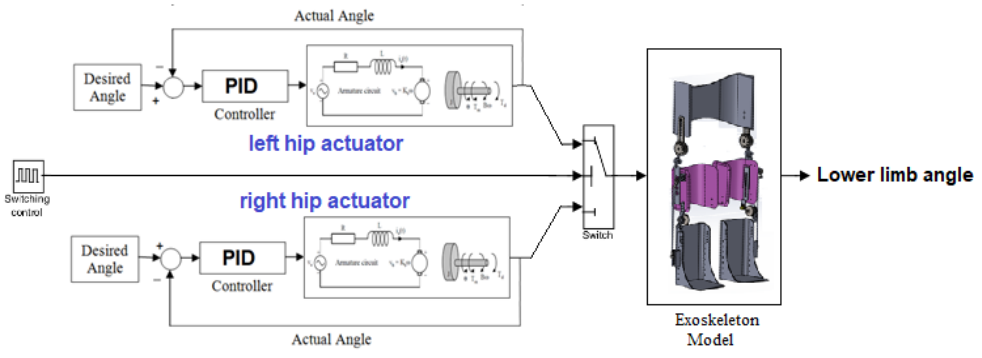

Fig. 7. Control structure of the proposed EM-HKAFO in simulation.

https://doi.org/10.24191/jmeche.v22i1.4553

Experimental setup and results for position tracking control of EM-HKAFO

Fig 8 and Fig 9 illustrate the experimental setup used for position tracking DC motor control with the actual exoskeleton, aimed at validating the simulated results. In this setup, a DC motor is integrated into the hip exoskeleton, functioning as the actuator to actuate the exoskeleton. The objective is to accurately track and control the position of the exoskeleton using the actuator. To achieve this, a joystick toggle switch as shown in Fig 9 is used as the control input for the validation process. The joystick toggle provides control signals along the *x*-axis for the right leg and the *y*-axis for the left leg of the exoskeleton. By toggling the joystick in different directions, users can command the exoskeleton to move accordingly. During the experiment, the desired angle is set to be 0.436 rad (25º) based on the study by Geonea & Tarnita (2017). When the joystick is switched on, the DC motor will follow the desired position set in the controller. The control system namely the PID controller, dynamically adjusts the DC motor's actions based on the joystick's position and the exoskeleton's feedback, ensuring precise and accurate position tracking.

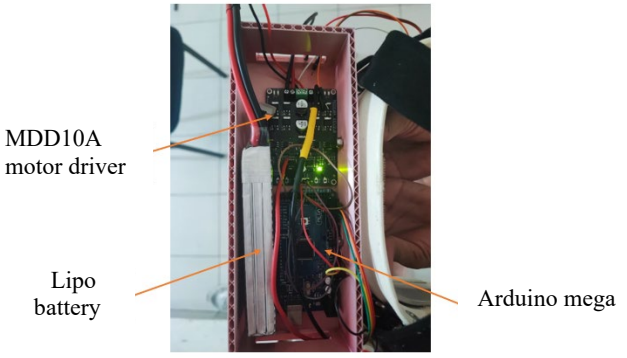

Fig. 8. Electronic parts to control DC motor.

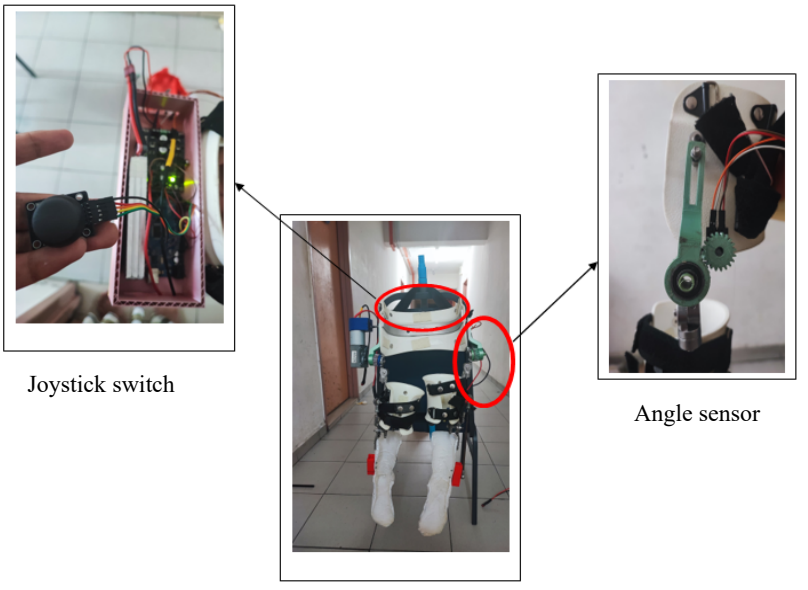

Fig. 9. Experimental setup for exoskeleton.

https://doi.org/10.24191/jmeche.v22i1.4553

The next assessment is evaluating the capability of the actuator to operate the exoskeleton. Fig 10(a) shows both simulation and experimental results for the right exoskeleton, focusing on the angular position of the hip. From the result, it can be seen that the experimental response has a similar trend in tracking the position of the exoskeleton as set in the controller command to control the overall lower limb movement. In terms of hip angle, the experimental result shows that the hip angle is approximately 0.37 rad where below the targeted angle of 0.436 rad. The result indicates that the actual exoskeleton successfully follows a similar trend as the simulated hip angle, demonstrating the effectiveness of the position-tracking control for the DC motor. However, there is a magnitude difference between the simulation and the experimental results of approximately 14%. Based on previous work done by Vidlak et al. (2021) showed that the maximum angle of the hip was 25º (0.436 rad). By comparing the result obtained in the experimental test and the previous result, it can be seen that the error is only 16% which is still in the acceptable range of error in the control system. Overall, the results demonstrate promising progress in the development of the exoskeleton and its position-tracking control, laying the foundation for potential future enhancements and applications in assisting individuals with mobility challenges.

For the left hip angle responses as illustrated in Fig 10(b), the experimental hip angle response is similar to the right hip angle set in the simulation with minor differences in time response. The left hip started to move at a time of 1.43 seconds based on the switch controller to wait for the complete cycle of the right hip movement. The experimental response is slightly delayed compared to the simulated response. The difference between the simulated and experimental left hip angle is approximately 14%. In both cases, the position-tracking control for the DC motors in the exoskeletons demonstrated promising results in tracking the desired hip angles. However, differences between the simulated and experimental outcomes highlight the complexities and challenges in accurately controlling the actual exoskeletons (Islam et al., 2020; Siviy et al., 2023). Certain factors are causing the error, such as mechanical tolerances and sensor inaccuracies (Qiu et al., 2023). To optimize the exoskeleton's performance and reduce the error, further investigation and adjustments might be required (Zou et al., 2024). Fine-tuning the control parameters, and enhancing sensor accuracy and dynamic factors in the actual system could help improve the tracking precision and minimize the difference between the simulated and actual hip angles (Fadzil et al., 2020). However, since the error in this study is less than 20%, it can be considered within the acceptable range (Aparow et al., 2014).

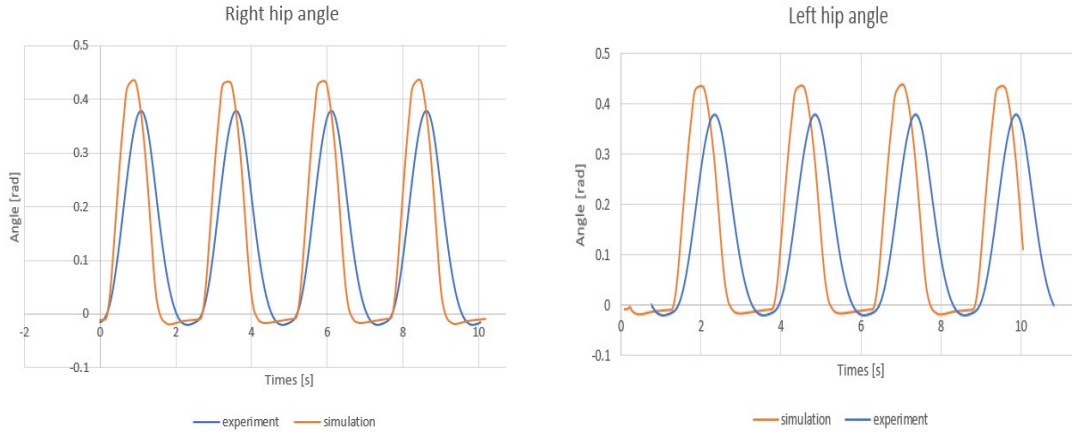

(a) (b)

Fig. 10. Hip angle simulation response with an actual EM-HKAFO hip angle response; (a) right hip exoskeleton and (b) left hip exoskeleton.

https://doi.org/10.24191/jmeche.v22i1.4553

CONCLUSION

In this study, a two-degree-of-freedom exoskeleton system was developed for controlling hip and knee angles using the Lagrange formulation. The system was integrated with a DC motor system through Matlab-Simulink to simulate the electromechanical hip-knee-ankle-foot orthosis (EM-HKAFO) response, aiming to mimic natural walking movements. The initial phase involved position tracking control of the DC motor, employing a combination of simulation and hardware-in-the-loop experiments to assess the actuator's ability to achieve the desired joint angles. The results from both simulation and experimentation indicated an acceptable error relative to the controller's command. The simulation results showed a mere 0.9% error in comparison to the desired angle, while the hardware-in-the-loop testing of the actual DC motor system yielded a 10% error against the desired angle. Subsequently, the development of the EM-HKAFO was carried out using a switching controller, merging the real exoskeleton and DC motor system in an experimental setting. This phase showed that the actual EM-HKAFO successfully tracked the desired walking path angle with a 14% error. To ensure smooth and coordinated motion, refinements to the controller may be necessary. This could encompass parameter fine-tuning and optimization methods to improve control performance. Moreover, the controller should take into account various factors such as inertia, acceleration, and deceleration to facilitate seamless transitions between different movements. By iteratively optimizing and considering external factors, it is conceivable to enhance the exoskeleton's performance leading to smoother and more natural movement. Advanced control techniques such as feedback control or predictive control can also be explored to further enhance the exoskeleton's responsiveness and movement coordination.

ACKNOWLEDGMENT

The research was conducted under the Self-Funded Research Grant SF0141-UPNM/2023/SF/TK/3 at the Faculty of Engineering, Universiti Pertahanan Nasional Malaysia. The authors also wish to acknowledge the support of the Pusat Pengurusan Penyelidikan & Inovasi, Universiti Pertahanan Nasional Malaysia for providing the financial assistance necessary for this publication.

CONFLICT OF INTEREST STATEMENT

All authors declare that they have no conflicts of interest.

AUTHORS' CONTRIBUTIONS

The authors confirm their contribution to the paper as follows: **HiLS setup, analysis of position tracking control using HiLS and manuscript preparation:** Zulkiffli Abd Kadir; **analysis of position tracking control by simulation and parameter optimization**: Muhammad Akhmal Hakim Alias, Khisbullah Hudha; **mathematical derivation and design**: Aina Nabila Azman. All authors reviewed the results and approved the final version of the manuscript.

REFERENCES

Abdul Saad, W. A., Mat Dzahir, M. A., Mohamed, H., Ahmad, Z. A., Mohamad, M., Mad Saad, S., & Mat

Dzahir, M. A. (2017). Posture detection on active and inactive vertebrae of spine biomechanics in critical daily activities. Journal of Mechanical Engineering, 4(2), 49–74.

Aparow, V. R., Hudha, K., Ahmad, F., & Jamaluddin, H. (2014). Model–in–the–loop simulation of gap and torque tracking control using electronic wedge brake actuator. International Journal of Vehicle Safety, 7(3-4), 390–408.

Ataabadi, P. A., Abbassi, A., Letafatkar, A., & Vanwanseele, B. (2022). The effects of foot orthosis and low-dye tape on lower limb joint angles and moments during running in individuals with pes planus. Gait and Posture, 96(2), 154–159.

Barrera Sánchez, A., Blanco Ortega, A., Martínez Rayón, E., Gómez Becerra, F. A., Abúndez Pliego, A., Campos Amezcua, R., & Guzmán Valdivia, C. H. (2022). State of the art review of active and passive knee orthoses. Machines, 10(10), 865.

Bortole, M., Anusha, V., Fangshi, Z., Juan, C. M., Gerard, E. F., Jose, L. P., & Jose, L. C. (2015). The H2 robotic exoskeleton for gait rehabilitation after stroke: Early findings from a clinical study. Journal of Neuroengineering and Rehabilitation, 12(1), 1-14.

Cao, W., Chen, C., Wang, D., Wu, X., Chen, L., Xu, T., & Liu, J. (2021). A lower limb exoskeleton with rigid and soft structure for loaded walking assistance. IEEE Robotics and Automation Letters, 7(1), 454–461.

Chen, B., Zhong, C. H., Zhao, X., Ma, H., Guan, X., Li, X., Liang, F. Y., Cheng, J. C. Y., Qin, L., Law, S. W., & Liao, W. H. (2017). A wearable exoskeleton suit for motion assistance to paralysed patients. Journal of Orthopaedic Translation, 11(C), 7–18.

Ekso Bionics (2024). The leader in exoskeleton technology. Ekso Bionics. https://eksobionics.com/

Emhemed, A. A. A., & Mamat, R. B. (2012). Modelling and simulation for industrial DC motor using intelligent control. Procedia Engineering, 41, 420–425.

Fadzil, W. F. A. W., Mazlan, M. A., Abdullah, A. H., Hanapiah, F. A., & Pangesty, A. I. (2020). Effects of infill density on 3D printed socket for transtibial prosthetic leg. Journal of Mechanical Engineering, 9(1), 229–238.

Gan, D., Qiu, S., Guan, Z., Shi, C., & Li, Z. (2016). Development of an exoskeleton robot for lower limb rehabilitation. International Conference on Advanced Robotics and Mechatronics (ICARM) (pp. 312–317), IEEE Publisher.

Gao, M., Wang, Z., Pang, Z., Sun, J., Li, J., Li, S., & Zhang, H. (2022). Electrically driven lower limb exoskeleton rehabilitation robot based on anthropomorphic design. Machines, 10(4), 266.

Geonea, I. D., & Tarnita, D. (2017). Design and evaluation of a new exoskeleton for gait rehabilitation. Mechanical Sciences, 8(2), 307–321.

Huamanchahua, D., Taza-Aquino, Y., Figueroa-Bados, J., Alanya-Villanueva, J., Vargas-Martinez, A., & Ramirez-Mendoza, R. A. (2021). Mechatronic exoskeletons for lower-limb rehabilitation: An innovative review. International IOT, Electronics and Mechatronics Conference (IEMTRONICS) (pp. 1–8). IEEE Publisher.

Islam, M. R., Brahmi, B., Ahmed, T., Assad-Uz-Zaman, M., & Rahman, M. H. (2020). Exoskeletons in upper limb rehabilitation: A review to find key challenges to improve functionality. In Boubaker, O. (Ed.), Control Theory in Biomedical Engineering (pp. 235–265). Academic Press.

https://doi.org/10.24191/jmeche.v22i1.4553

Jin, X., Zhu, S., Zhu, X., Chen, Q., & Zhang, X. (2017). Single-input adaptive fuzzy sliding mode control of the lower extremity exoskeleton based on human–robot interaction. Advances in Mechanical Engineering, 9(2), 1-9.

Kadir, Z. A., Azman, A. N., Hudha, K., Amer, N. H., Zubir, A. R., & Alawi, A. H. M. (2023). Kinematic analysis of double pendulum for exoskeleton walking aid. Conference on Systems, Process & Control (ICSPC) (pp. 96-100). IEEE Publisher.

Khalid, U. B., Naeem, M., Stasolla, F., Syed, M. H., Abbas, M., & Coronato, A. (2024). Impact of AI-powered solutions in rehabilitation process: Recent improvements and future trends. International Journal of General Medicine, 17, 943-969.

Kobayashi, T., Orendurff, M. S., Hunt, G., Gao, F., LeCursi, N., Lincoln, L. S., & Foreman, K. B. (2019). The effects of alignment of an articulated ankle-foot orthosis on lower limb joint kinematics and kinetics during gait in individuals post-stroke. Journal of Biomechanics, 83, 57–64.

Li, H., Yu, H., Chen, Y., Tang, X., Wang, D., Meng, Q., & Du, Q. (2022). Design of a minimally actuated lower limb exoskeleton with mechanical joint coupling. Journal of Bionic Engineering, 19(2), 370–389.

Mayag, L. J. A., Múnera, M., & Cifuentes, C. A. (2022). Human-in-the-loop control for agora unilateral lower-limb exoskeleton. Journal of Intelligent and Robotic Systems, 104(1), 3.

Qiu, S., Pei, Z., Wang, C., & Tang, Z. (2023). Systematic review on wearable lower extremity robotic exoskeletons for assisted locomotion. Journal of Bionic Engineering, 20, 436–469.

Shi, D., Zhang, W., Zhang, W., & Ding, X. (2019). A review on lower limb rehabilitation exoskeleton robots. Chinese Journal of Mechanical Engineering, 32, 1–11.

Siviy, C., Baker, L. M., Quinlivan, B. T., Porciuncula, F., Swaminathan, K., Awad, L. N., & Walsh, C. J. (2023). Opportunities and challenges in the development of exoskeletons for locomotor assistance. Nature Biomedical Engineering, 7(4), 456–472.

Tang, X., Wang, X., Ji, X., Zhou, Y., Yang, J., Wei, Y., & Zhang, W. (2022). A wearable lower limb exoskeleton: Reducing the energy cost of human movement. Micromachines, 13(6), 900.

Vidlak, M., Gorel, L., Makys, P., & Stano, M. (2021). Sensorless speed control of brushed DC motor based on new current ripple component signal processing. Energies, 14(17), 5359.

Wang, T., Zhang, B., Liu, C., Liu, T., Han, Y., Wang, S., Ferreira, J. P., Dong, W., & Zhang, X. (2022). A review on the rehabilitation exoskeletons for the lower limbs of the elderly and the disabled. Electronics, 11(3), 388.

Yan, Z., Han, B., Du, Z., Huang, T., Bai, O., & Peng, A. (2021). Development and testing of a wearable passive lower-limb support exoskeleton to support industrial workers. Biocybernetics and Biomedical Engineering, 41(1), 221–238.

Zou, C., Peng, Z., Zhang, L., Mu, F., Huang, R., & Cheng, H. (2024). Optimization-based adaptive assistance for lower limb exoskeleton robots with a robotic walker via spatially quantized gait. IEEE Transactions on Automation Science and Engineering, 1-13.

https://doi.org/10.24191/jmeche.v22i1.4553